Lab on a Chip

Drop-of-Sample Rheometry of Biological Fluids by Noncontact Acoustic Tweezing Spectroscopy

Journal:	*Lab on a Chip*
Manuscript ID	LC-ART-04-2022-000356.R1
Article Type:	Paper
Date Submitted by the Author:	01-Jul-2022
Complete List of Authors:	Kasireddy, Nithya; Tulane University, Department of Biomedical Engineering Orie, Jeremy; Tulane University, Department of Biomedical Engineering Khismatullin, Damir; Tulane University, Department of Biomedical Engineering

ARTICLE

Drop-of-Sample Rheometry of Biological Fluids by Noncontact Acoustic Tweezing Spectroscopy

Received 00th April 20xx,
Accepted 00th April 20xx

DOI: 10.1039/x0xx00000x

Nithya Kasireddy,*[a] Jeremy C. Orie [a] and Damir B. Khismatullin *[a]

Knowledge of rheological properties, such as viscosity and elasticity, is necessary for efficient material processing and transportation as well as biological analysis. Existing rheometers operate with large sample volume and induce sample contact with container or device walls, which are inadequate for rheological analysis of sensitive fluids limited in availability. In this work, we introduce acoustic tweezing spectroscopy (ATS), a novel noncontact rheological technique that operates with a single 4-6μl drop of fluid sample. In ATS, a sample drop is acoustically levitated and then exposed to a modulated acoustic signal to induce its forced oscillation. The time-dependent sample viscosity and elasticity are measured from the resulting drop response. The ATS measurements of polymeric solutions (dextran, xanthan gum, gelatin) agrees well with previously reported data. The ATS predicts the shear viscosity of blood plasma increases from 1.5cP at 1.5min of coagulation onset to 3.35cP at 9min, while its shear elastic modulus grows from a negligible value to 10.7Pa between 3.5min and 6.5min. Whole blood coagulation increases viscosity from 5.4cP to 20.7cP and elasticity from 0.1Pa to 19.2Pa at 15min. In summary, ATS provides the opportunity for sensitive small-volume rheological analysis in biomedical research and medical, pharmaceutical, and chemical industries.

Introduction

The ability of complex fluids to flow and deform under applied stresses depends on rheological properties such as viscosity and elasticity. Knowledge of these properties is necessary for processing of polymeric and biological materials[1-10], oil and gas production and transportation[11, 12], and diagnosis and treatment monitoring based on biological fluid analysis[1, 13-16], to name a few. Majority of existing rheometers operate with a relatively large sample volume (>0.5ml) and induce sample contact with device walls[17-21]. The reduction in sample volume and avoiding the wall-slip artifacts and contact induced sample contamination[22, 23] are needed for safe and reliable analysis of biological fluids.

The sample volume issue has been addressed in several alternate techniques[24-26], including the electrodynamic acoustic shear wave method[27], liquid-filament micro-rheometry[28], optical based laser speckle rheology[29-31] and microfluidics[32-34]. They have been successfully applied for rheological measurements of hydrogels, synovial fluid, saliva, bronchial sputum, and blood. However, these techniques are limited in the viscosity values they can measure and shear rates they can operate, but most importantly they further exacerbate the issue of sample wall contact due to, for example, an increase in the surface area to volume ratio.

The containerless measurement requires levitation of a liquid sample. In acoustic tweezing technology[35], rheological properties are assessed from a single liquid drop with volume as small as 4μl acoustically levitated in air. This technology addresses both the sample volume and sample wall contact issues in rheological analysis. It infers the sample properties by quasi-static and oscillatory techniques. The quasi-static method, in which sample deformation is induced by slowly varying acoustic pressure, is highly sensitive to sample elasticity changes and has been shown to be effective for sample firmness measurement during coagulation or polymerization[35, 36]. In the oscillatory method, the sample deformation (shape oscillation) is achieved by amplitude modulation of the input pressure. The sample rheological properties are then measured from either the free decay response[37, 38] or the forced oscillation amplitude frequency response. The latter approach known as "Acoustic Tweezing Spectroscopy" (ATS) is the focus of this study. The free decay approach, referred to as "Drop Oscillation Rheometry" (DOR)[37] is usable for damping ratio lower than 0.1, limiting its application to small changes in viscosity and elasticity. Operating the acoustic tweezing device in the forced oscillation regime addresses this issue.

This work introduces the ATS as a single-drop non-contact technique for time-dependent viscoelastic measurements of polymer solutions and biological fluids. In particular, using the viscosity standards and theoretical analysis, the ATS output was corelated with sample viscoelasticity. The obtained relationships were applied and validated for measurement of rheological properties of dextran, xanthan gum and gelatin

[a] Department of Biomedical Engineering, Tulane University, 6823 St. Charles Avenue, New Orleans, Louisiana, 70118, USA.
*Corresponding author. Email: damir@tulane.edu
†Electronic Supplementary Information (ESI) available: Sec. S1. Theory for drop shape oscillation. Sec. S2. Peak frequency for medical viscosity standard fluids. See DOI: 10.1039/x0xx00000x

solutions. The ATS was then used to measure coagulation induced changes in viscosity and elasticity of whole blood and blood plasma.

Materials and Methods

Reagents

Medical viscosity standard (MVS) fluids with viscosities of 1.2cP, 1.6cP, 2.0cP, 4.0cP, 6.0cP and 10cP, xanthan gum from Xanthomonas campestris, and gelatin from porcine skin with gel strength 200 were purchased from Millipore Sigma (Burlington, Massachusetts). Dextran with molecular weight of 2,000kDa and 35 to 45kDa was purchased from Millipore Sigma and US Biological Life Sciences (Salem, Massachusetts), respectively. Dextran was mixed with phosphate-buffered saline (PBS, Thermo Fisher Scientific, Waltham, Massachusetts) to attain (1-5% w/v concentration). Xanthan gum was mixed with distilled water (0.1-0.3% w/v concentration) and then allowed to dissolve at room temperature for 2-3 hours. (2-4% w/v) gelatin-in-water mixtures were kept in a water bath at 37˚C for at least 30 minutes to dissolve.

Control normal, level 1 human plasma in lyophilized form and aPTT-XL (ellagic acid) reagent were purchased from Thermo Fisher Scientific. Calcium chloride ($CaCl_2$) was purchased from Millipore Sigma. 0.2M solution of $CaCl_2$ was prepared by mixing with PBS. Similarly, blood plasma was prepared by mixing its lyophilized powder with PBS. The plasma was either used immediately or aliquoted into small batches that were stored in -80˚C. Whole blood was collected from healthy volunteers in sodium citrate tubes under protocol number 520566 approved by Tulane University Institutional Review Board on 09-23-20 and the volunteers provided informed consent.

Washed pooled sheep red blood cells (RBCs, 10%) were purchased from Rockland Immunochemicals (Gilbertsville, PA). 1:1 ratio of the 10% washed RBCs and phosphate buffered saline (PBS) were mixed to prepare 5% RBC solution. PBS was used as the control group (0% RBC).

Experimental Setup

A custom acoustic tweezing system used in this study has the following components (Fig. 1A, Ref. 35): 1) an acoustic levitator consisting of a transducer with a resonance frequency of 29.5 kHz; 2) a reflector placed at half wavelength from the transducer surface; 3) two function waveform generators (33220A, Agilent, Santa Clara, California); 4) a wideband power amplifier (7500, Krohn-Hite Corporation, Brockton, Massachusetts); 5) an area scan digital camera (acA1920-25um, Basler, Ahrensburg, Germany) or a high-speed digital video camera (HotShot HS MegaX3CC, NAC Image Technology, Tokyo, Japan); 6) a focused light source (Odepro KL52Plus, Odepro Technology, Shenzhen, China); 7) a photodetector (DET100A, Thorlabs, Newton, New Jersey); 8) a data acquisition system (cDAQ-9171 with NI-9239 C voltage input module, National Instruments, Austin, Texas) and 9) a cool mist humidifier (AquaOasis, Monsey, New York). The carrier signal was created by one of the function generators. The swept modulation of the signal amplitude was achieved by the second function generator. The resulting driving signal, shown in Fig. 1B, was further amplified, and sent to the transducer. Without modulation, the driving signal generates a standing acoustic wave between the transducer and the reflector which enables levitation of a liquid drop near the pressure node. The signal modulation causes drop deformation (acoustic tweezing) in the form of quadrupole shape oscillation (Fig. 1C). The modulated signal was swept from 150 Hz to 50 Hz at a rate of 10 Hz/sec at a modulation depth β of 10% using a custom VI program (LabView, National Instruments). The frequency sweep was repeated every 30 seconds. Note that sweeping below the frequency of 40Hz causes instability of the drop and inability to maintain its levitation at constant acoustic pressure. For the same reason, it is difficult to achieve forced shape oscillation of low surface tension fluids, e.g., silicone oil, that have the natural frequency below that critical frequency. The levitation of such drops requires a reduction of acoustic pressure (carrier signal amplitude) at which the response of the drop to the swept modulation is much weaker and may lead to the drop falling[39, 40]. Therefore, we decided to calibrate our data using medical viscosity standard fluids that have a higher surface tension.

The change in drop height during frequency sweep (Fig. 1D) was measured from voltage output of the photodetector, as previously described[41], using DAQExpress software version 4.0 (National Instruments). Additionally, images of the drop were captured by a digital camera using Pylon Viewer (Basler AG) during every sweep (one image per sweep) and analyzed by a custom edge detection algorithm in MATLAB 2020b (Mathworks, Natick, Massachusetts) to obtain the instantaneous equivalent radius R and aspect ratio b/a of the drop. The drop height data were post-processed in MATLAB by using a bandpass filter that kept the frequency components within the swept frequency range and removed the low and high frequency noise components that may arise due to external factors such as surrounding air movement and output electrical power fluctuations. Also, the time scale was converted into the frequency scale based on the rate of sweeping. The total peak-to-peak amplitude of the drop deformation was calculated at swept frequencies as a difference between the upper and lower envelopes of the drop height. The peak-to-peak amplitude versus frequency curve is referred to as “amplitude-frequency response” (AFR) of the drop (Fig. 1E). See the electronic supplementary information for a video demonstrating an ATS experiment.

Experimental Procedure

To initiate the intrinsic pathway of coagulation, 18µl whole blood, 18µl freshly reconstituted blood plasma, or 18µl frozen blood plasma after thawing in a water bath was mixed with 6µl aPTT-XL containing 0.2M $CaCL_2$. $CaCl_2$ was not added to the control group. In each experiment, a 6 µl drop of a test fluid (MVS, dextran, xanthan gum, gelatin, blood plasma, or whole blood) was deployed into the acoustic tweezing device using a 0.2-10µL single channel electronic pipette (CAPP Maestro M10-1, Nordhausen, Germany). Note that in all the experiments with

gelatin, the sample was taken from a heated water bath and placed immediately into the device operated at room temperature. The cooling of gelatin sample inside the device led to its gelation.

At least half an hour before an experiment, the humidifier located near the device was turned on to maintain humidity of surrounding air at 90% or above. Based on data obtained by the quasi-static method, the levitated drop decreased its radius by less than 5% in 20 minutes of tweezing at this humidity level. During the drop deployment, the device was operated without amplitude modulation. The modulation sweep was then introduced, and the resulting drop response (AFR) was measured as explained above. The following parameters were extracted from each AFR curve (Fig. 1E): peak frequency f_{peak}, peak amplitude A_{peak}, area under the curve (AUC), amplitude at the lowest modulation frequency A_{min}, amplitude at the highest modulation frequency A_{max}. The quality factor (QF) was calculated as the ratio of the peak frequency and the difference between the frequencies at half peak amplitude, $f_{1/2,\text{left}}$ and $f_{1/2,\text{right}}$ (Fig. 1E):

$$\text{QF} = \frac{f_{\text{peak}}}{f_{1/2,\text{right}} - f_{1/2,\text{left}}} \quad (1)$$

The angular peak frequency $\omega_{\text{peak}} = 2\pi f_{\text{peak}}$. The sample viscoelasticity was measured by the **resonant** technique using the QF, A_{peak}, and ω_{peak} or the **nonresonant** technique using AUC and A_{min}. All the AFR parameters showed linear dependence on the drop aspect ratio, which was accounted for, along with the drop volume, when calculating the normalized values of the parameters:

$$P^{(n)} = \frac{P - c}{b / a\sqrt{R^3}}. \quad (2)$$

Here P and $P^{(n)}$ are the parameter values before and after the normalization and c is the y-intercept of the parameter vs. aspect ratio curve.

Viscosity Measurement Based on the properties of the MVS fluids, the theoretical AFR curves were generated using the following equation for the amplitude of forced drop oscillation [see Eq. (S11) in Sec. S1.3†]:

$$x = \frac{A}{\sqrt{(8\sigma - \rho\omega^2 R^3)^2 + (8\mu\omega R)^2}}, \quad (3)$$

where x is the drop oscillation amplitude, A the driving amplitude, ω the angular modulation frequency, σ the surface tension, ρ the density, and μ the viscosity of the fluid. From the theoretical AFR curves, we obtained the theoretical A_{peak} and QF for MVS fluids. To obtain the theoretical AUC, the trapezoidal numerical integration of Eq. (3) was performed. For all of the three parameters, correlation analysis was conducted between the theoretical and experimental values for the MVS fluids to get the correction factors for the theoretical data. Uncorrected theoretical values were then obtained for a wide range of viscosities. The correction factors were applied to the theoretical A_{peak}, QF and AUC vs. viscosity data to obtain the viscosity calibration curves for these parameters.

Elasticity Measurement In the resonant method, the elastic modulus G was obtained from the peak frequency using the following formula [see Eq. (S7) in Sec. S1.1†]:

$$G = \frac{\rho R^2[(\omega_{peak}^{(n)})^2 - \omega_L^2]}{10}, \quad \omega_L = \sqrt{\frac{8\sigma}{\rho R^3}}. \quad (4)$$

Here ω_L is the Lamb frequency for the quadrupole shape oscillation of the drop.

In the nonresonant method, G was estimated from the A_{min} data using the empirical relationship established based on the gelatin G values measured by the resonant method:

$$G = G_0 + (35 - G_0)\exp(-40A_{\text{min}}), \quad (5)$$

where G_0 is the initial elasticity value. It should be noted that the peak frequency is independent on the viscosity as illustrated in Fig. S1†.

Statistical and Corelation Analysis

The data were analyzed by GraphPad Prism software (GraphPad software, San Diego, CA). The p value was calculated by Mann-Whitney nonparametric t-test and set at <0.05 for a statistically significant difference. Data normality was confirmed by the Shapiro-Wilk test. Linear correlation was established by using the Pearson coefficient of correlation R_{p}.

Results

Fig. 2 shows the AFR curves for water, low and high molecular weight dextran solutions, MVS fluids, and control and recalcified blood plasmas. There were multiple peaks in the water and low molecular weight (35 – 45 kDa) dextran solution AFRs (Fig. 2A, green and blue). These peaks appeared because of energy transfer from quadrupole shape oscillation into other modes of oscillation, e.g., drop twisting, when the drop approached resonance. They were not observed for high molecular weight (2,000kDa) dextran (Fig. 2A, pink). There are two reasons by which this behavior can be explained: 1) viscosity difference between the low and high molecular weight dextran solutions; and 2) fiber structure formation in the high molecular weight dextran solution. As seen in Fig. 2B, an increase in fluid viscosity reduces the number of peaks and/or the region of instability around the resonant peak. The instability region width was ~21.5Hz for MVS 1.2, but it reduced to ~14.8Hz, 13.1Hz, 12.9Hz and 8.2Hz for MVS 1.6, 2, 4, and 6, respectively. MVS 10 had a single peak. The presence of structure inside the drop also had a strong effect on the drop behavior near resonance. For example, blood plasma had a single peak in the AFR curve despite having the same viscosity as MVS 1.2 (Fig. 2C). This is explained by the presence of large macromolecules in plasma such as albumin, fibrinogen and globulins. Adding red blood cells to a saline solution at a hematocrit of as low as 5% caused the multiple peak disappearance (see Fig. 6 below). When comparing the AFR curves for control and recalcified blood plasmas (Fig. 2D), it is clearly seen that coagulation caused a decrease in peak amplitude and an increase in resonance frequency. The rate of change in peak amplitude in recalcified plasma was higher than

in control plasma (Fig. 2D, solid and dashed lines) due to the increased viscous damping during coagulation. There was a small shift in peak frequency in control plasma due to drop evaporation. A much larger change in peak frequency was seen in recalcified plasma which is a result of the elasticity increase. The peak nearly disappeared at 5min since initiation of coagulation indicating the necessity of using the nonresonant method at later times.

Fig. 3 illustrates the effect of viscosity on resonant (A_{peak}, QF) and nonresonant (AUC) AFR properties. The A_{peak} and QF had strong correlation (R_{p} = 0.89 - 0.91) and AUC had a very strong correlation (R_{p} = 0.94) with viscosity (Fig. 3A,C,E). The slightly reduced sensitivity of the resonant parameters was a direct result of the multiple peak appearance in low viscosity fluids (Fig. 2B). As seen in Fig. 3(B,D,F), there exists an excellent agreement between the normalized experimental and theoretical values of these parameters (R_{p} = 0.99 for A_{peak} and AUC, and R_{p} = 0.98 for QF), described by the following correction equations:

$$\begin{aligned} A_{\mathrm{peak}}^{(\mathrm{exp,n})} &= 0.53 A_{\mathrm{peak}}^{(theor,\mathrm{n})} - 0.03, \\ \mathrm{QF}^{(\mathrm{exp,n})} &= 2.5\,\mathrm{QF}^{(theor,\mathrm{n})} - 8.4, \\ \mathrm{AUC}^{(\mathrm{exp,n})} &= 1.6\,\mathrm{AUC}^{(theor,\mathrm{n})} - 24. \end{aligned} \quad (6)$$

Equations (6) were used to generate the viscosity calibration curves.

By applying the calibration curves to experimental data, we measured the viscosities of the following polymer solutions: dextran solutions, which are Newtonian fluids (no elasticity[35]), xanthan gum solutions, which show time-independent viscoelastic behavior[42], and gelatin solutions whose viscoelastic properties change during gelation[43] (Fig. 4). The normalized AUC, A_{peak}, and QF significantly changed ($p < 0.0001$, $R_{\mathrm{p}} = 0.95$-0.99) with dextran concentration (Fig. 4A-C). The dextran solution viscosity measured from these parameters agreed well with previously reported values[44] (Fig. 4D). The best agreement was obtained for the nonresonant method (AUC), which predicted that the 3%, 4% and 5% dextran solutions had the mean viscosity of 5.39, 8.11 and 11.3 cP, respectively (solid bars). These values deviated from the reported values (dashed lines) by respectively 2.18%, 1.44% and 3.76%, all within the 95% confidence interval of the mean. In the resonant method, viscosities predicted by QF were outside the confidence interval for the 3% and 5% dextran, but no such deviation was observed for viscosities assessed from A_{peak}. Based on this analysis, the nonresonant method was applied to measure viscosities of other fluids.

The normalized AUC for xanthan gum decreased with an increase in gum concentration from 0.1% to 0.3% but it did not change with time (Fig. 4E). The latter is expected because of fixed viscosity of xanthan gum. The mean viscosity of 0.1%, 0.2%, and 0.3% xanthan gum estimated from the calibration curves was 9.12, 12.5, and 15.6 cP, respectively (Fig. 4F). The percent difference between our measurement and the reported values[45] was 2.5% for 0.1%, 0.2% for 0.2% and 1.3% for 0.3% solution. These differences were within the 95% confidence interval of the mean.

The gelatin normalized AUC also decreased with gelatin concentration, but it reduced with time due to viscosity increase during the gelation process (Fig. 4G). Within 20 minutes of acoustic tweezing, the viscosity increased from 10.4 cP to 41.9 cP for 2% gelatin, from 14.0 cP to 52.05 cP for 3% gelatin, and from 16.1 cP to 60.1 cP for 4% gelatin (Fig. 4H).

Fig. 5 shows the elasticity measurement of xanthan gum and gelatin solutions by ATS. The peak frequency (resonant technique) increased with the gum concentration between 0.1% and 0.3% but did not change with time (Fig. 5A). This resulted in the following mean values of elasticity: 0.22 Pa for 0.1%, 0.58 Pa for 0.2%, and 1.3 Pa for 0.3% xanthan gum (Fig. 5B). These values deviated from the reported values[46, 47] (dashed lines) by respectively 0.6%, 7.2% and 7.5%, all within the 95% confidence interval.

As seen in Fig. 5C, the peak frequency and thus elasticity increased with time and gelatin concentration, while A_{min} showed the opposite trend (Fig. 5D). Note that an increase in gelatin viscosity caused the peak disappearance in the AFR curve at ~11.5 min for 3% and 8 min for 4% gelatin at which the resonant technique became unusable. Due to a lack of elasticity standards, we had to rely on the resonant G data to obtain the calibration curve for the nonresonant method. As evident from Fig. 5E, there exists an exponential relationship between A_{min} and G in which only the initial elasticity value G_0 depends on the gelatin concentration [cf. Eq. (5)]. This relationship was used to predict the gelatin elasticity before and after the peak disappearance (Fig. 5F). A good match was observed for the elasticity values measured by the resonant (filled symbols) and nonresonant methods (hollow symbols).

Once validated, we have applied the ATS technique to measure viscosity of RBC solutions and changes in viscoelasticity of blood plasma and whole blood during coagulation. Fig. 6 shows results from ATS experiments performed using sheep RBC solutions with different hematocrits. As seen in Fig. 6(A), drops in the control group had multiple peaks in the amplitude frequency response (AFR, black dashed line). Adding a small amount of RBCs (5% RBC) caused the multiple peak disappearance (pink solid line). The further increase in hematocrit (10%) led to a reduction in peak amplitude due to an increase in viscosity (green, dash dotted line). Thus, the ATS can detect the presence of cellular components in the sample drop and measure its volume fraction through analysis of the number and amplitude of the AFR peaks. There was a significant difference between the normalized area under the curve (AUC) for all the three groups (Fig. 6B). The mean viscosity of 0%, 5%, and 10% sheep RBC solutions estimated using ATS were 1.0cP, 2.5cP, and 2.8cP, respectively (Fig. 6C).

Control anticoagulated blood plasma had negligible shear elasticity G and its mean shear viscosity μ was ~1.5cP, as previously reported[48, 49] (Fig. 7A,B, circles). When the plasma was recalcified, G increased to its plateau value of 10.7 Pa between 3.5 min and 6.5 min (Fig. 7A, squares). The μ of recalcified plasma started to increase at about 1.5 min and reached its highest value of 3.35cP at 9 min (Fig. 7B, squares). The elasticity of recalcified whole blood increased from 0.1 Pa

at 3 min to 19.2 Pa at 15 min (Fig. 7C). Its viscosity increased from about 5.4 cP before the onset of coagulation[49, 50] to 20.7 cP at 15 min of coagulation (Fig. 7D). The change in elasticity of coagulating blood plasma is identical to the mechanical tweezograph reported in Ref. 36. It should be noted that the sample drop elasticity is proportional to the drop radius squared, according to Eq. (4). Therefore, we anticipate that the elasticity values obtained by our single drop technique will be less than measured by rotational rheometry and other large sample volume techniques. Recent rotational rheometry measurements of 160µl blood plasma samples (effective radius of ~3.37mm)[51] predict that the plasma elasticity reaches the value of 98.2 Pa when fully clotted. The effective radius of our blood plasma samples was ~3 times smaller than the sample size in that study. Thus, if rotational rheometry were applied to 6µl samples, the elasticity is projected to be 11.0 Pa, which lies within the confidence interval of the mean of our measurement (10.7 Pa).

Discussion

The ability of this method to detect rheological properties of fluids with such a small volume provides an opportunity for testing fluids where availability is limited, difficult to extract, or extremely expensive to produce. For instance, rheological analysis of pharmaceutical products is routinely used for assessment of their dosage and stability[6, 52-54]. Reduction in sample volume significantly decreases the cost of this analysis [55, 56] and can bring down drug development costs, particularly for expensive protein- and antibody-based biopharmaceutical formulations[57].

Biological fluids that can be collected from small animals are very limited, and some of them are difficult to extract from humans. The measurement of their rheological properties is essential for assessment of their function in normal and diseased states. For example, rheological changes in synovial fluid are an early biomarker of arthritis and mixed connective tissue disease [13, 58, 59]. Up to 4µl and 200µl of synovial fluid can be extracted from small (mice) and large (canine) animals for biomarker analysis[60], which is not sufficient for traditional rheological analysis. The human knee contains 0.5-4ml[61] synovial fluid, which is often extracted during the total knee arthroplasty[62] but collection of such a large volume is not advisable during early stages of arthritis. Small volume rheology is also required for pathological analysis of the vitreous, a fluid that fills the eye[63-67] as well as severity analysis of lung infection[68] and vocal disorders[69]. The total vitreous volume in human eyes is about 4ml[70] while the collected volume of human laryngeal mucus ranges from 10µl to 1.8ml[69]. The ATS enables safe and reliable analysis of these fluids.

The flow of blood in both small and large vessels critically depends on its rheological properties. Many pathophysiological conditions developed in the cardiovascular system are associated with changes in blood rheology including blood viscosity and elasticity. Whole blood and blood plasma viscosities are well recognized biomarkers of ischemic heart disease, stroke, myocardial infarction and hypertension[71-75]; hematological disorders[76]; cancer[77, 78]; diabetes[79]; hypercoagulable state in smokers[80]; and aging[81]. Viscoelastic analysis of whole blood and blood plasma[82-84] is performed to assess blood coagulation status and predict bleeding/thrombosis risks in critical care patients[85-89], patients on anticoagulant therapy[90], patients with diseases impacting the coagulation system[91-95] and patients with clotting disorders such as hemophilia and thrombophilia[96, 97].

Coagulation analysis is currently done by contact techniques that operate with relatively large volumes of blood, which lead to diagnostic errors[98] and may cause iatrogenic anemia in small children and the elderly[99-101]. Due to the safety concerns, coagulation tests are not performed as often as required in these groups of patients. With minimal sample volume (a single drop of blood) and noncontact measurements, the acoustic tweezing technology enables safe, fast, and reliable analysis of blood viscosity and coagulation in vulnerable patients. The emerging application of small volume coagulation analysis is a quick finger prick test for risk assessment of infectious disease, particularly COVID-19 which severity is associated with the hypercoagulable state[102, 103].

The results presented in this work (Figs. 2 and 6) indicate that the ATS technique can detect the presence of particles or large macromolecules within the sample drop, in addition to viscoelastic measurements. This can potentially be used for structural analysis of biological fluids including detection of high molecular weight compounds, concentration measurement of blood plasma proteins, and cell counting.

Conclusions

This work introduces a novel non-contact technique (acoustic tweezing spectroscopy or ATS) for dynamic rheological measurements of polymeric and biological fluids. The ATS uses only a single drop of fluid sample (4-6µl) per measurement, and viscosity and elasticity data produced by this technique agreed well with the previously reported data for dextran, xanthan gum, blood plasma and whole blood. The ATS addresses the issue of sample contact with container walls which may lead to artificial changes in rheological properties of highly sensitive biological materials. Our future work will be focused on clinical validation of the ATS-based coagulation analysis; using ATS for blood viscosity analysis in cardiovascular disease; testing this technique on pharmacological formulations and other biological fluids; and its expansion for fluid structural analysis.

Author Contributions

N.K. contributed towards conceptualization, data curation, formal analysis, investigation, methodology, software, validation, visualization, and writing including editing. J.C.O. contributed towards software development. D.B.K. contributed towards conceptualization, funding acquisition, methodology, project administration, resources, supervision, validation, and writing including reviewing and editing.

Conflicts of interest

N.K. and D.B.K. have the following conflicts of interest to disclose: N.K. owns equity and has an employment at Levisonics Inc. She is also an inventor listed on the patent PCT/US21/15336 (pending). D.B.K. owns equity in Levisonics Inc. He is also an inventor on patents PCT/US14/55559 (issued), PCT/US2018/014879 (issued) and PCT/US21/15336 (pending). J.C.O. declares no conflict of interest.

Acknowledgements

This study has been supported by U.S. National Science Foundation (Grants No. 1438537 and 1843479), American Heart Association (Grants No. 13GRNT17200013 and 20PRE35210991), and Tulane University intramural grants. The authors thank Daishen Luo for acoustic tweezing device setup; Erika Chelales for help with experimental data analysis; and R. Glynn Holt, Donald Gaver, and Amina Rafique for helpful discussions.

References

1. A. Borzacchiello, L. Ambrosio, P. Netti and L. Nicolais, in *Tissue Engineering and Novel Delivery Systems*, CRC Press, 2003, pp. 341-361.
2. J. M. Dealy and K. F. Wissbrun, in *Melt Rheology and Its Role in Plastics Processing*, Springer, 1999, pp. 567-600.
3. G. Tabilo-Munizaga and G. V. Barbosa-Cánovas, *Journal of food engineering*, 2005, **67**, 147-156.
4. D. Gómez-Díaz and J. M. Navaza, *Journal of Food Engineering*, 2003, **56**, 387-392.
5. S. O. Ilyin and L. A. Strelets, *Energy & Fuels*, 2018, **32**, 268-278.
6. D. J. Mastropietro, R. Nimroozi and H. Omidian, *J. Dev. Drugs*, 2013, **2**, 1-6.
7. D. S. Jones, A. D. Woolfson and A. F. Brown, *International journal of pharmaceutics*, 1997, **151**, 223-233.
8. E. G. Rippie and D. W. Danielson, *Journal of pharmaceutical sciences*, 1981, **70**, 476-482.
9. L. Ambrosio, A. Borzacchiello, P. Netti and L. Nicolais, *Journal of Macromolecular Science—Pure and Applied Chemistry*, 1999, **36**, 991-1000.
10. S. Santesson and S. Nilsson, *Anal Bioanal Chem*, 2004, **378**, 1704-1709.
11. X.-X. Feng, J. Zhang, D. Zhang and J.-Y. Xu, *Journal of Petroleum Science and Engineering*, 2019, **176**, 141-149.
12. A. M. Saad, S. Aime, S. C. Mahavadi, Y.-Q. Song, T. W. Patzek and D. Weitz, 2020.
13. H. Fam, J. Bryant and M. Kontopoulou, *Biorheology*, 2007, **44**, 59-74.
14. C.-S. Rhee, Y. Majima, J.-S. Cho, S. Arima, Y.-G. Min and Y. Sakakura, *Archives of Otolaryngology–Head & Neck Surgery*, 1999, **125**, 101-105.
15. L. Dintenfass, *Angiology*, 1974, **25**, 365-372.
16. N. Lemonne, K. Charlot, X. Waltz, S. K. Ballas, Y. Lamarre, K. Lee, R. Hierso, C. Connes, M. Etienne-Julan, M. Romana and P. Connes, *Haematologica*, 2015, **100**, e383-386.
17. L. H. O. Hellström, M. A. Samaha, K. M. Wang, A. J. Smits and M. Hultmark, *Measurement Science and Technology*, 2014, **26**, 015301.
18. A. Magnin and J. Piau, *Journal of Non-Newtonian Fluid Mechanics*, 1990, **36**, 85-108.
19. T. Kiljański, *Rheologica acta*, 1989, **28**, 61-64.
20. G. M. Eccleston and N. E. Hudson, *J Pharm Pharmacol*, 2000, **52**, 1223-1232.
21. A. Allahham, D. Mainwaring, P. Stewart and J. Marriott, *J Pharm Pharmacol*, 2004, **56**, 709-716.
22. A. S. Yoshimura and R. K. Prud'homme, *Journal of Rheology*, 1988, **32**, 575-584.
23. W. E. Krause, E. G. Bellomo and R. H. Colby, *Biomacromolecules*, 2001, **2**, 65-69.
24. S. Gupta, W. S. Wang and S. A. Vanapalli, *Biomicrofluidics*, 2016, **10**, 043402.
25. C. J. Pipe and G. H. McKinley, *Mechanics Research Communications*, 2009, **36**, 110-120.
26. J. D. Martin, J. N. Marhefka, K. B. Migler and S. D. Hudson, *Adv Mater*, 2011, **23**, 426-432.
27. E. K. Reichel, A. Abdallah, C. Feichtenschlager, M. Kramer, A. Moritz and B. Jakoby, *Procedia engineering*, 2015, **120**, 171-174.
28. A. Bazilevsky, V. Entov and A. Rozhkov, *Fluid Dynamics*, 2011, **46**, 613-622.
29. Z. Hajjarian and S. K. Nadkarni, *Annu Int Conf IEEE Eng Med Biol Soc*, 2011, **2011**, 5746-5748.
30. Z. Hajjarian, H. T. Nia, S. Ahn, A. J. Grodzinsky, R. K. Jain and S. K. Nadkarni, *Sci Rep*, 2016, **6**, 37949.
31. M. M. Tripathi, Z. Hajjarian, E. M. Van Cott and S. K. Nadkarni, *Biomed Opt Express*, 2014, **5**, 817-831.
32. N. Srivastava, R. D. Davenport and M. A. Burns, *Anal Chem*, 2005, **77**, 383-392.
33. Y. J. Kang, S. Y. Yoon, K. H. Lee and S. Yang, *Artif Organs*, 2010, **34**, 944-949.
34. J. Lee and A. Tripathi, *Anal Chem*, 2005, **77**, 7137-7147.
35. R. G. Holt, D. Luo, N. Gruver and D. B. Khismatullin, *J Thromb Haemost*, 2017, **15**, 1453-1462.
36. D. Luo, E. M. Chelales, M. M. Beard, N. Kasireddy and D. B. Khismatullin, *Anal Bioanal Chem*, 2021, **413**, 3369-3379.
37. V. Ansari Hosseinzadeh and R. G. Holt, *Journal of Applied Physics*, 2017, **121**, 174502.
38. P. A. Evans, K. Hawkins, M. Lawrence, M. S. Barrow, P. R. Williams and R. L. Williams, *Clin Hemorheol Microcirc*, 2008, **38**, 267-277.
39. E. H. Trinh and C. J. Hsu, *J Acoust Soc Am*, 1986, **79**, 1335-1338.
40. P. Singha, N. K. Nguyen, J. Zhang, N. T. Nguyen and C. H. Ooi, *Colloid Surface A*, 2021, **627**.
41. V. A. Hosseinzadeh and R. G. Holt, *Journal of Applied Physics*, 2017, **121**.
42. L. Fagioli, L. Pavoni, S. Logrippo, C. Pelucchini, L. Rampoldi, M. Cespi, G. Bonacucina and L. Casettari, *Journal of food science*, 2019, **84**, 65-72.
43. M. Djabourov, J. Leblond and P. Papon, *Journal de Physique*, 1988, **49**, 333-343.
44. S. Kuenzi, E. Meurville and P. Ryser, *Sensor Actuat B-Chem*, 2010, **146**, 1-7.
45. D. Li, X. Shao, J. B. Bostwick and X. Xuan, *Microfluidics and Nanofluidics*, 2019, **23**, 1-11.
46. M. M. Mrokowska and A. Krzton-Maziopa, *Sci Rep*, 2019, **9**, 7897.

47. J. Carmona, P. Ramírez, N. Calero and J. Muñoz, *Journal of Food Engineering*, 2014, **126**, 165-172.
48. J. Harkness, *Biorheology*, 1971, **8**, 171-193.
49. C. A. Trejo-Soto, E. Costa-Miracle, A. Rodríguez-Villarreal, J. Cid, M. Castro, T. Alarcón and A. Hernández-Machado, 2018.
50. A. Rasyid, J. Misbach, J. S. Purba, I. S. Timan, L. Sukrisman, M. Mansyur, E. Yudiarsah and Suroto, *Acta Med Indones*, 2014, **46**, 226-232.
51. S. Liu, G. Bao, Z. Ma, C. J. Kastrup and J. Li, *bioRxiv*, 2021.
52. P. C. Acharya, D. Suares, S. Shetty, C. Fernandes and R. K. Tekade, in *Dosage Form Design Considerations*, Elsevier, 2018, pp. 549-597.
53. J. Aho, J. P. Boetker, S. Baldursdottir and J. Rantanen, *Int J Pharm*, 2015, **494**, 623-642.
54. S. A. Schildcrout, *J Pharm Pharmacol*, 1984, **36**, 502-505.
55. A. Saluja and D. S. Kalonia, *J Pharm Sci*, 2005, **94**, 1161-1168.
56. J. Jezek, M. Rides, B. Derham, J. Moore, E. Cerasoli, R. Simler and B. Perez-Ramirez, *Adv Drug Deliv Rev*, 2011, **63**, 1107-1117.
57. V. Bansode, P. Gupta, N. Kateja and A. S. Rathore, *Journal of Chemical Technology & Biotechnology*, 2021.
58. J. E. Gomez and G. B. Thurston, *Biorheology*, 1993, **30**, 409-427.
59. T. Conrozier, P. Mathieu, E. Vignon, M. Piperno and M. Rinaudo, *Clin Exp Rheumatol*, 2012, **30**, 729-734.
60. D. R. Seifer, B. D. Furman, F. Guilak, S. A. Olson, S. C. Brooks, 3rd and V. B. Kraus, *Osteoarthritis Cartilage*, 2008, **16**, 1532-1538.
61. V. B. Kraus, T. V. Stabler, S. Kong, G. Varju and G. McDaniel, *Osteoarthritis and cartilage*, 2007, **15**, 1217-1220.
62. S. Honsawek, A. Tanavalee and P. Yuktanandana, *Arch Med Res*, 2009, **40**, 590-594.
63. P. Sharif-Kashani, J. P. Hubschman, D. Sassoon and H. P. Kavehpour, *J Biomech*, 2011, **44**, 419-423.
64. B. Lee, M. Litt and G. Buchsbaum, *Biorheology*, 1994, **31**, 339-351.
65. B. Lee, M. Litt and G. Buchsbaum, *Biorheology*, 1994, **31**, 327-338.
66. B. Lee, M. Litt and G. Buchsbaum, *Biorheology*, 1992, **29**, 521-533.
67. F. Watts, L. E. Tan, C. G. Wilson, J. M. Girkin, M. Tassieri and A. J. Wright, *Journal of Optics*, 2013, **16**, 015301.
68. X. Murgia, A. M. Kany, C. Herr, D. K. Ho, C. De Rossi, R. Bals, C. M. Lehr, A. K. H. Hirsch, R. W. Hartmann, M. Empting and T. Rohrig, *Sci Rep*, 2020, **10**, 16502.
69. G. Peters, O. Wendler, D. Bohringer, A. O. Gostian, S. K. Muller, H. Canziani, N. Hesse, M. Semmler, D. A. Berry, S. Kniesburges, W. Peukert and M. Dollinger, *Appl Sci (Basel)*, 2021, **11**.
70. J. Sebag, *The vitreous: structure, function, and pathobiology*, Springer Science & Business Media, 2012.
71. M. Woodward, A. Rumley, H. Tunstall-Pedoe and G. D. Lowe, *Br J Haematol*, 1999, **104**, 246-257.
72. E. Ernst, A. Matrai and M. Marshall, *Stroke*, 1988, **19**, 634-636.
73. E. H. Ozcan Cetin, M. S. Cetin, U. Canpolat, E. Kalender, S. Topaloglu, D. Aras and S. Aydogdu, *Med Princ Pract*, 2015, **24**, 444-450.
74. S. Chien, *Biorheology*, 1986, **23**, 633-653.
75. T. Khodabandehlou, M. Boisseau and C. Le Devehat, *Clinical hemorheology and microcirculation*, 2004, **30**, 307-312.
76. S. Chien, S. Usami and J. F. Bertles, *J Clin Invest*, 1970, **49**, 623-634.
77. G. F. von Tempelhoff, L. Heilmann, G. Hommel and K. Pollow, *Semin Thromb Hemost*, 2003, **29**, 499-513.
78. G. F. von Tempelhoff, F. Nieman, L. Heilmann and G. Hommel, *Clin Hemorheol Microcirc*, 2000, **22**, 107-130.
79. G. Lowe, J. Lowe, M. Drummond, S. Reith, J. Belch, C. Kesson, A. Wylie, W. Foulds, C. Forbes and A. MacCuish, *Diabetologia*, 1980, **18**, 359-363.
80. J. Levenson, A. C. Simon, F. A. Cambien and C. Beretti, *Arteriosclerosis*, 1987, **7**, 572-577.
81. M. J. Simmonds, H. J. Meiselman and O. K. Baskurt, *J Geriatr Cardiol*, 2013, **10**, 291-301.
82. R. J. Luddington, *Clin Lab Haematol*, 2005, **27**, 81-90.
83. S. Collins, C. MacIntyre and I. Hewer, *AANA J*, 2016, **84**, 129-134.
84. A. Saleem, C. Blifeld, S. A. Saleh, D. H. Yawn, M. L. Mace, M. Schwartz and E. S. Crawford, *Ann Clin Lab Sci*, 1983, **13**, 115-124.
85. F. Herbstreit, E. M. Winter, J. Peters and M. Hartmann, *Anaesthesia*, 2010, **65**, 44-49.
86. E. Jensen, S. Andreasson, A. Bengtsson, H. Berggren, R. Ekroth, L. E. Larsson and J. Ouchterlony, *Ann Thorac Surg*, 2004, **77**, 962-967.
87. A. Shah, S. McKechnie and S. Stanworth, *Semin Thromb Hemost*, 2016, **42**, 95-101.
88. M. Levi and B. J. Hunt, *J Thromb Haemost*, 2015, **13**, 1960-1967.
89. B. Nascimento, M. Al Mahoos, J. Callum, A. Capone, J. Pacher, H. Tien and S. Rizoli, *Transfusion*, 2012, **52**, 7-13.
90. B. Salmela, L. Joutsi-Korhonen, E. Armstrong and R. Lassila, *Semin Thromb Hemost*, 2012, **38**, 23-30.
91. M. Mohren, K. Jentsch-Ullrich, M. Koenigsmann, S. Kropf, E. Schalk and G. Lutze, *Int J Hematol*, 2016, **103**, 189-195.
92. H. A. Pearson, *Pediatr Res*, 2002, **52**, 979-992.
93. R. Marcucci, F. Sofi, S. Fedi, B. Lari, I. Sestini, A. P. Cellai, R. Pulli, G. Pratesi, C. Pratesi, G. F. Gensini and R. Abbate, *J Thromb Haemost*, 2005, **3**, 502-507.
94. J. D. Banga, *Semin Vasc Med*, 2002, **2**, 75-86.
95. D. Noubouossie, N. S. Key and K. I. Ataga, *Blood Rev*, 2016, **30**, 245-256.
96. M. Chitlur and G. Young, *Semin Hematol*, 2016, **53**, 40-45.
97. I. Jennings and P. Cooper, *Br J Biomed Sci*, 2003, **60**, 39-51.
98. G. P. Gravlee, S. Arora, S. W. Lavender, S. A. Mills, A. S. Hudspeth, A. R. Cordell, R. L. James, J. K. Brockschmidt and J. J. Stuart, *Ann Thorac Surg*, 1994, **58**, 216-221.
99. S. M. Emani, *Semin Thromb Hemost*, 2019, **45**, 302-307.
100. S. R. Howie, *Bull World Health Organ*, 2011, **89**, 46-53.
101. T. S. Dharmarajan and C. Pitchumoni, in *Geriatric Gastroenterology*, Springer, 2012, pp. 261-269.
102. S. Tal, G. Spectre, R. Kornowski and L. Perl, *Acta Haematol*, 2020, **143**, 417-424.
103. F. A. Klok, M. Kruip, N. J. M. van der Meer, M. S. Arbous, D. Gommers, K. M. Kant, F. H. J. Kaptein, J. van Paassen, M. A. M. Stals, M. V. Huisman and H. Endeman, *Thromb Res*, 2020, **191**, 148-150.

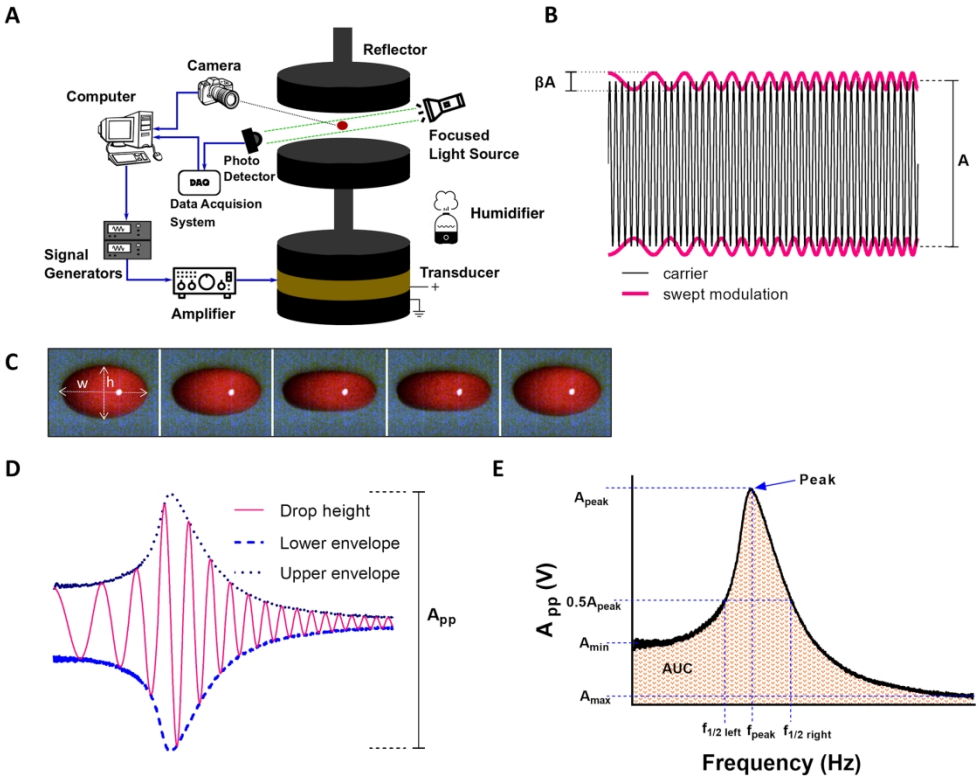

Fig. 1. (A) Schematic of the acoustic tweezing apparatus. (B) The drop was driven into shape oscillations by the sinusoidal carrier wave (black) with swept amplitude modulation (pink). (C) Images of an oscillating blood drop during acoustic tweezing. (D) Driving signal induced change in drop height (pink), as measured from the photo-detector output. Dark and light blue curves are the upper and the lower envelopes of the drop response. (E) Amplitude-frequency response of the drop obtained from the envelope data in (D) with the following parameters extracted: area under the curve (AUC), f_{peak} , A_{peak}, A_{min}, A_{max}, $f_{1/2\ right}$, and $f_{1/2\ left}$.

222x178mm (300 x 300 DPI)

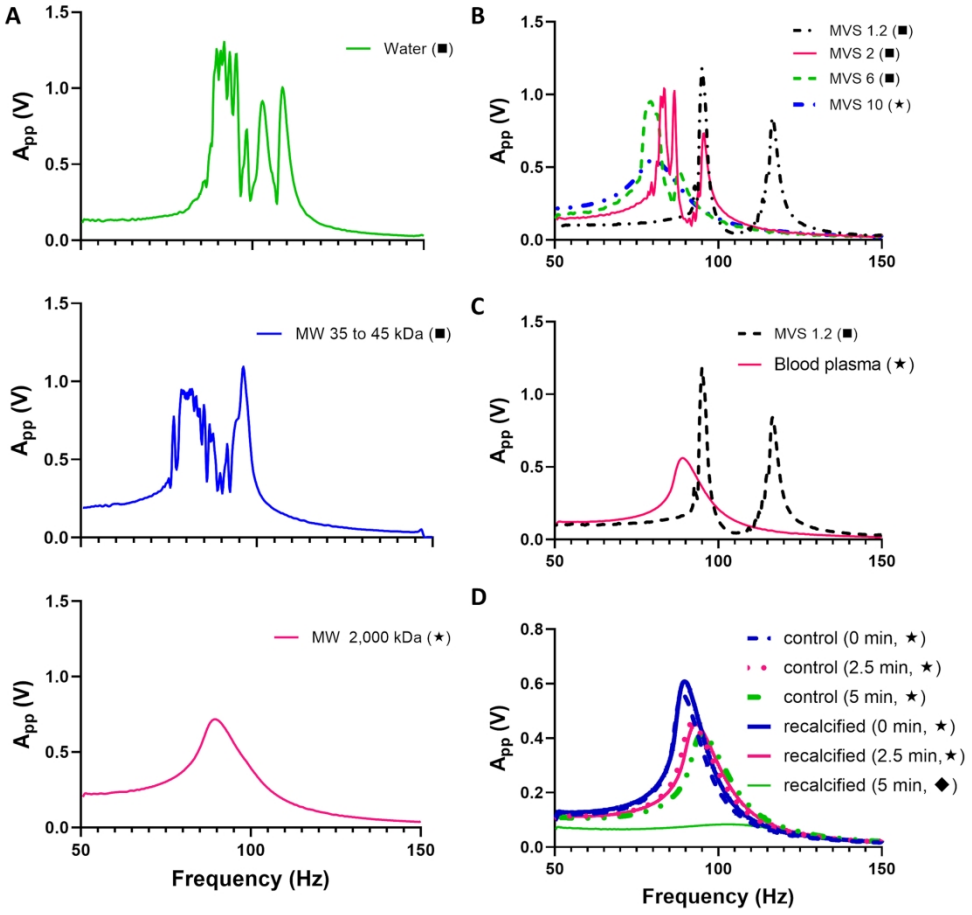

Fig. 2. Amplitude frequency response (AFR) of (A) water (green) and 5% (w/v) dextran of molecular weights of 35 to 45kDa (blue) and 2,000kDa (pink); (B) MVS fluids with viscosity 1.2cP (black), 2.0cP (pink), 6.0cP (green), and 10cP (blue); (C) MVS with viscosity 1.2cP (green) and commercial blood plasma (pink); (D) untreated blood plasma (dashed lines) and blood plasma treated with aPTT-XL and CaCl2 (solid lines) at time 0 min (blue), 2.5 min (pink) and 5 min (green). □ represents an AFR curve with multiple peaks due to instability, ★ represents a smooth ARF curve, and ◆ represents an AFR curve in the non-resonance phase.

214x207mm (300 x 300 DPI)

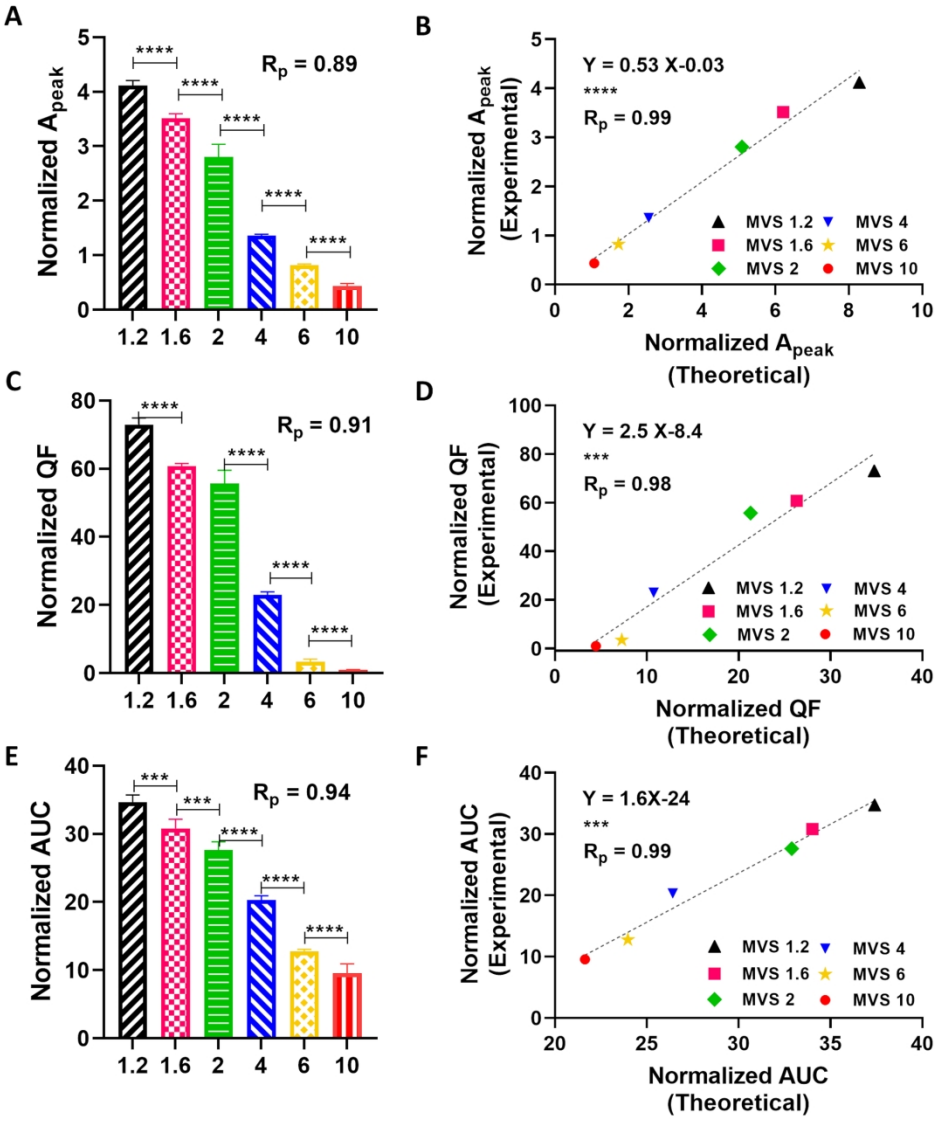

Fig. 3. Normalized peak amplitude (A), quality factor (C), AUC (E) for MVS fluids with viscosity 1.2 cP (black), 1.6 cP (pink), 2.0 cP (green), 4.0 cP (blue), 6.0 cP (yellow) and 10 cP (red). Also shown are theoretical versus experimental correlation curves for peak amplitude (B), quality factor (D) and area under the curve (F). Sample size n = 9. ***$p < 0.001$, ****$p < 0.0001$.

186x216mm (300 x 300 DPI)

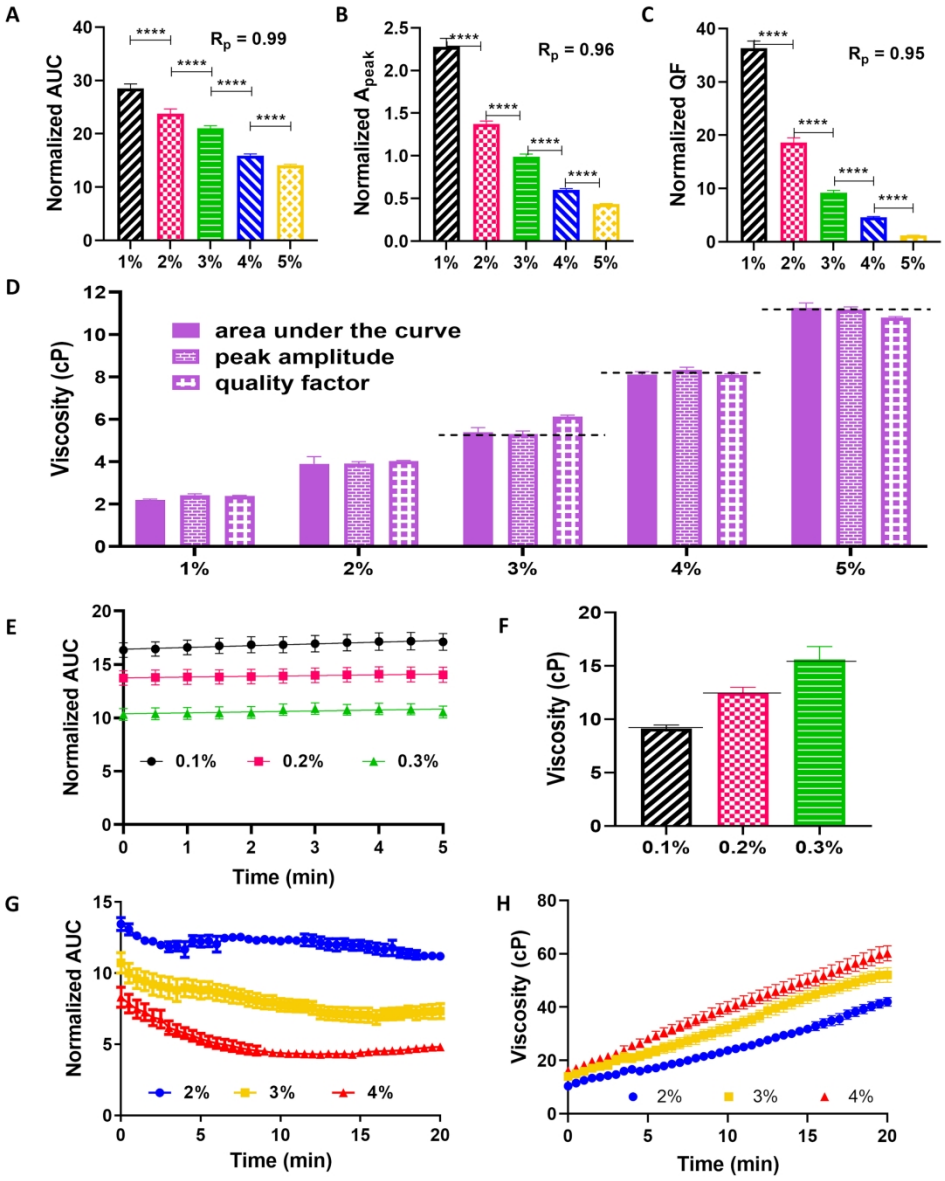

Fig. 4. Normalized AUC (A), peak amplitude (B), quality factor (C), and (D) viscosity measured by the nonresonant (solid bar) and resonant (horizontal stripes, checkerboard) ATS for 1% (black, n = 10), 2% (pink, n = 10), 3% (green, n = 25), 4% (blue, n = 25), and 5% (red, n = 26) high molecular weight (2,000 kDa) dextran solutions. Also shown are (E) Normalized AUC vs. time and (F) viscosity for 0.1% (black, n = 17), 0.2% (pink, n = 17), and 0.3% (green, n = 16) xanthan gum solutions. (G, F) are the normalized AUC and viscosity vs. time for 2% (blue, n = 4), 3% (yellow, n = 5), and 4% (red, n = 4) gelatin solutions. The viscosity of xanthan gum and gelatin solutions was measured by the nonresonant method. Black dashed lines in (D) and black solid lines in (F) are reported reference values of viscosity for dextran and xanthan gum solutions. ****$p < 0.0001$.

231x285mm (300 x 300 DPI)

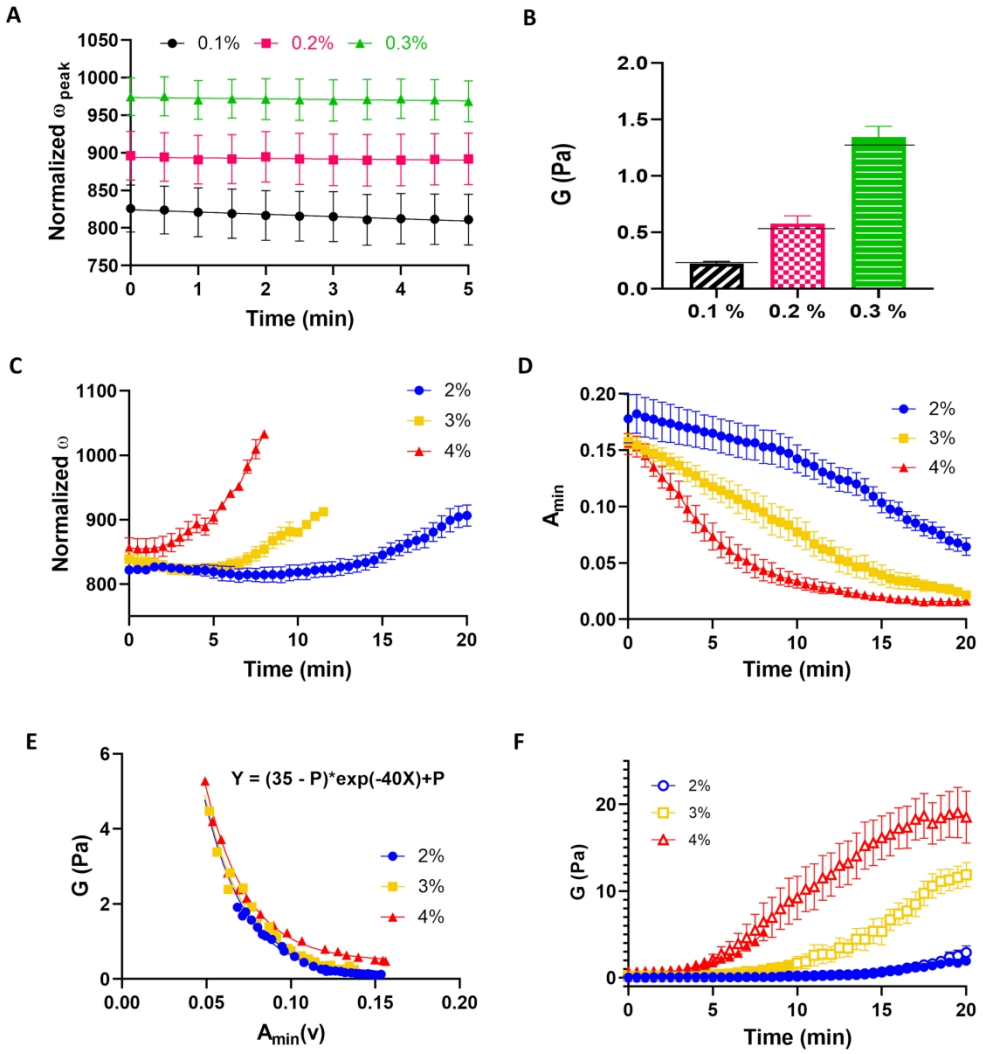

Fig. 5. Normalized ω_{peak} (A) and elastic modulus G (B) for 0.1% (black, n = 17), 0.2% (pink, n = 17), and 0.3% (green, n = 16) xanthan gum solutions. (C, D) show normalized ω_{peak} and A_{min} vs. time for 2% (blue, n = 4); 3% (yellow, n = 5); and 4% (red, n = 4) gelatin solutions. In (E, F), elastic modulus G of gelatin solutions is plotted as a function of A_{min} and time, based on measurements by the resonant (solid symbols) and nonresonant (hollow symbols) methods. Black solid lines in (B) are reported reference values of xanthan gum solution elasticity.

225x243mm (300 x 300 DPI)

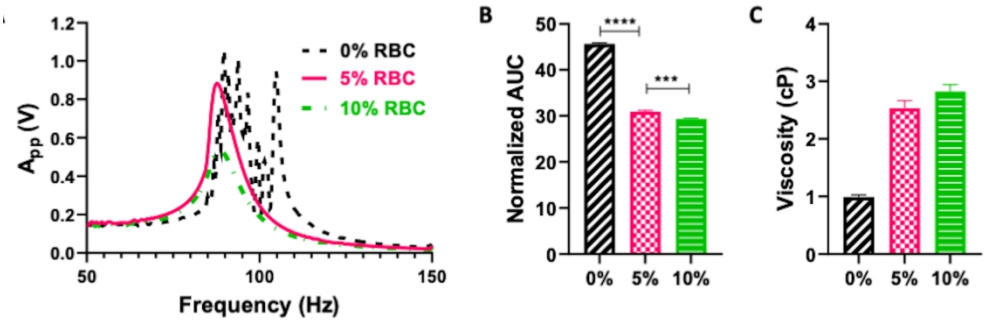

Fig. 6. (A) Amplitude frequency response, (B) Normalized AUC, and (C) viscosity of PBS with 0% (black), 5% (pink) and 10% (green) sheep RBCs, measured by ATS. Sample size n = 10 to 13. ***$p < 0.001$, ****$p < 0.0001$.

219x76mm (300 x 300 DPI)

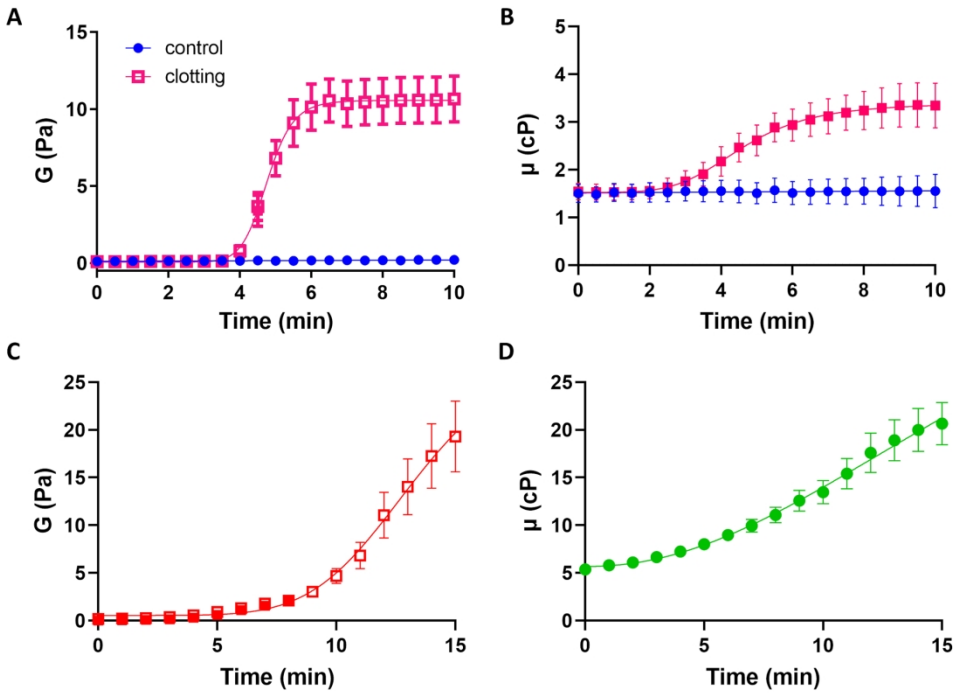

Fig. 7. Elastic modulus G (A) and viscosity μ (B) vs. time for control anticoagulated plasma (blue, n = 5) and plasma treated with aPTT-XL and $CaCl_2$ (pink, n = 10). (C, D) show G (red, n = 16) and μ (green, n =18) vs. time for whole blood treated with aPTT-XL and $CaCl_2$. In (A, C), hollow and solid symbols are the data produced by the nonresonant and resonant methods, respectively.

213x157mm (300 x 300 DPI)